HiSST: 3rd International Conference on
High-Speed Vehicle Science Technology
14 -19 April 2024, Busan, Korea

Longitudinal Acoustic Field in a Two-Phase Ramjet: Numerical Simulation and Acoustics Models

E. Bekaert [1], A. Genot [1], T. Le Pichon [1] and T. Schuller [2]

Abstract

Thermoacoustic instabilities are recurrent in ramjets and may cause thermal and mechanical fatigue, as well as engine extinction. To study and predict the development of such instabilities resulting from the coupling between pressure and heat release rate fluctuations, the internal acoustic field itself needs to be characterized and predicted. As a first step, a description of the acoustic field in a two-inlet side-dump ramjet in a liquid-fuelled configuration is proposed relying on numerical simulations. Two predominant oscillation modes are identified by spectral analysis. Their origin and spatial structure are investigated comparing the numerical results with a linear acoustics reduced-order model for pressure fluctuations. Lastly, complex phenomena observed by numerical simulation are studied by an *ad hoc* correction of the linear acoustic model introducing a harmonic translation velocity to the mode shape, replicating the trends observed numerically.

Keywords: *Ramjet, acoustic modes, thermoacoustic instabilities, reduced-order model, translation*

Nomenclature

Latin
A_O – outlet admittance
A_I – inlet admittance
a – speed of sound
k – wave number
l_a – acoustic length
M – Mach number
P_- – arbitrary amplitude of the wave
p – pressure

Greek
β – reflection coefficient
Z – temporal part
Y – spatial part
ω – angular frequency
$\dot{\omega}_T$ – heat release rate

Subscripts
0 – mean flow
1 – fluctuating part
n – corresponding mode

Acronyms
ZDES – Zonal Detached Eddy Simulation

1. Introduction

Similar to other propulsion devices such as rockets or gas turbines, ramjets are prone to combustion instabilities resulting in high-amplitude oscillations of physical quantities (pressure, velocities etc.), leading to premature extinctions, chamber damages or, in worst cases, destruction of the system. The prediction of combustion instabilities through empirical methods is challenging due to the complexity of the various physical phenomena involved in their occurrence, as well as their multitude of physical and temporal scales. Instabilities driven by the coupling between the internal acoustic field and the unsteady combustion dynamics within the combustor are called thermoacoustic instabilities. Rayleigh [1] was the first to describe the coupling between a heating source and an internal acoustic field, suggesting energy transfers when they oscillate in phase. His description was later theorized by the Rayleigh criterion which quantifies the stability of the system, involving pressure and heat release rate

[1] *DMPE, ONERA, Université Paris Saclay, 91120, Palaiseau, France* erwin.bekaert@onera.fr, aurelien.genot@onera.fr, thomas.le_pichon@onera.fr
[2] *Institut de Mécanique des Fluides de Toulouse, IMFT, Université de Toulouse, CNRS, Toulouse, France,* thierry.schuller@imft.fr

fluctuations, respectively p_1 and $\dot{\omega}_{T_1}$:

$$\frac{1}{T}\int_V \int_T p_1 \, \dot{\omega}_{T_1} \, dVdt > \text{acoustic losses} > 0 \quad (1)$$

where physical quantities ϕ are decomposed as the sum of their mean and fluctuating part as follows: $\phi(x,t) = \phi_0(x) + \phi_1(x,t)$, V is the domain volume and T a period of oscillation. If this criterion is verified, an instability with self-sustained oscillations is growing and conversely, the system tends to stability when the thermoacoustic coupling is weaker than the system losses.

As highlighted by Culick [2] and Liewen [3], thermoacoustic modes are often considered close to natural acoustic modes of the system. Ghirardo *et al.* [4] supported this thesis by listing twenty references from the literature and establishing the ratio between thermoacoustic modes and natural acoustic mode frequencies. They noticed a frequency shift of approximately 10% of the values of natural eigenmode frequencies, implying that the origin of the thermoacoustic modes resides mostly in natural geometric acoustic modes impacted by the unsteady heat release.

There are two main geometrical configurations of ramjets: the coaxial dump combustor and the side dump combustor. In the first configuration, air is coaxially injected upstream the combustion chamber [5,6] causing a sudden expansion of the flow section at the junction between the air inlet and the combustor. In the second configuration, the combustor is a cavity with a nozzle at its exit where air is injected laterally. There can be two lateral air inlets aligned [7], successive [8] or opposed [9,10] inducing different flow topologies.

Thermoacoustic instabilities have been identified in the ONERA experimental bench named Research Ramjet (in French *Statoréacteur de Recherche* (SdR)) [9,11]. It is a two-inlet side-dump ramjet combustor with square cross-section in the air inlet and combustion chamber which can either be operated with gaseous or liquid fuel injection, respectively propane or kerosene. Roux [12] conducted a Large Eddy Simulation (LES) of the one-phase configuration Research Ramjet in a geometric configuration close to the current one. Through spectral analysis of the acoustic field in its operational case, Roux corroborated the existence of two predominant low-frequency longitudinal modes, as experimentally demonstrated by Reichstadt [11]. He pointed out the complex modal structure of these modes and identified the second mode as a combustor half-wave natural acoustic mode. Similar complex modal structures were observed experimentally and by a linear thermoacoustic model by Crump *et al.* [5]. Their conclusions highlight the dependence of the acoustic field on the flow in the combustor and boundary conditions, especially at the air inlet.

An attempt is made in this study to characterize the complexity of the longitudinal acoustic field inside the liquid-fuelled Research Ramjet and bring elements of comprehension on the origins of this complexity. In particular, the spectral distribution and structure of the acoustic modes are investigated through numerical simulation and reduced-order models in order to corroborate previous observations [5,12] in the case of a two-phase flow with liquid fuel in a side-dump ramjet. The contributions of this study aim to enhance the understanding of the acoustics in a ramjet to enable an optimal reproduction of pressure fluctuations p_1, especially within the combustor, for an optimal $p_1 \, \dot{\omega}_{T_1}$ coupling to model the thermoacoustic behavior of the system.

At first, a description of the acoustics in the system through the mean and fluctuating fields is provided, relying on the temporal and spectral analysis of a three-dimensional Zonal Detached Eddy Simulation (ZDES)[13] of the Research Ramjet. The origin of predominant acoustic modes is then investigated based on a comparison of the modal structure obtained by a linear reduced-order acoustics model with the numerical simulation. Eventually, an *ad hoc* correction to the previous model is proposed to bring elements of comprehension on the origin of complex trends observed by numerical simulation.

2. Description of the acoustic field in the liquid-fuelled Research Ramjet

2.1. Computational methodology and flow topology

A three-dimensional reactive numerical simulation of the full-scale two-phase Research Ramjet has been performed using ONERA multi-physics CFD code CEDRE [14]. The Research Ramjet operates as follows: air is injected at the extremity of the two inlet ducts and then passes through sonic throats inducing a shock train in each duct. Air is convected towards the combustor, a spray of liquid kerosene

is injected and a combustion reaction takes place in the combustor, both upstream and downstream of the jet interaction zone. Burnt gases are convected towards the exit choked nozzle.

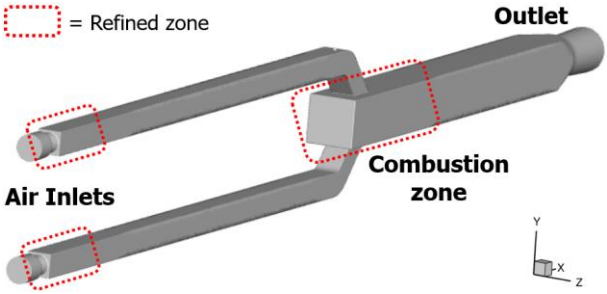

Fig. 1: 3D view of the ONERA Research Ramjet

The unstructured 12M elements mesh used for the simulation is refined to 1mm in high gradient zones, namely the shock train zones and the combustion zone in the upstream portion of the combustor. Two CEDRE solvers are coupled: the eulerian solver CHARME [14] for compressible flows and the lagrangian solver SPARTE [15] for the liquid fuel phase.

A Zonal Detached Eddy Simulation [13] approach with a DDES [16] formulation is used to model turbulence, allowing a $k-\omega$ SST RANS approach on the attached flow zones and a LES approach in detached zones. The blending function switching from RANS to LES was developed by Fan *et al.* [17]. A two-step chemical scheme for the air-kerosene reaction model [18] and a dynamic thickened flame model are used to model combustion.

Concerning numerical schemes in the CHARME solver, due to the presence of shocks in the flow, the spatial discretization is ensured by a 2nd order MUSCL-type method with multislope reconstruction [19] with Van Leer's limiter [20] for convective fluxes and a second-order centered scheme for the diffusive fluxes. A HLLC solver is used to solve the Riemann problems at each element face. For the temporal discretization, a time step of 4×10^{-7} s and a 1st order implicit scheme have shown optimal computational time while ensuring good stability.

The initial temperature of air at the inlet is 752K and kerosene droplets are injected at 300K upstream of the combustor with a diameter of the order of 1×10^{-4}m. All walls are treated adiabatically with a rebound condition for the fuel droplets. Since the latter are injected at different temperatures and velocities from the gaseous flow, there are convective effects. The spherical fuel droplets have heat exchanges with the flow and evaporate. Both Nusselt and Sherwood numbers are expressed with the empirical Ranz-Marshall law [21] to take those effects into account. Due to the small size of the droplets, conductive effects inside the droplets are considered infinitely fast making the internal temperature uniform. Finally, due to the difference of velocity between the flow and the droplets, shear forces acting on the latter force it to fragment. This phenomenon is characterized by the dimensionless critical Weber number above which droplets break up, it is set at $We_c = 12$ [22].

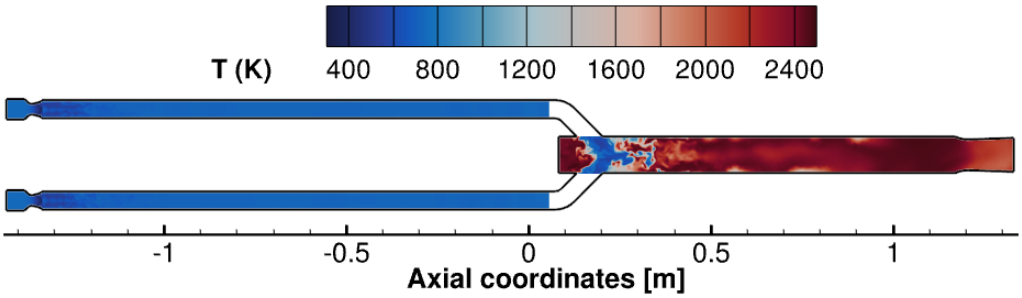

Fig. 2: Instantaneous temperature field in the median plane along the z-axis.

After achieving convergence of the simulation to pass transient phenomena, a simulated physical time of 0.238 s is used in this study. Two combustion zones are identified, aligning with both experimental [11] and numerical [12] observations of the one-phase configuration of the Research Ramjet. Fig. 2 depicts an instantaneous temperature field in the air inlets and in the combustion chamber in the median plane along the z-axis. The main combustion zone is located downstream the interaction zone of the two cold jets. The second combustion zone is situated upstream the jet interaction zone, within the dome. This is a recirculation zone with low axial velocities and elevated temperatures resulting from the mixing of burnt gases. Since the speed of sound a_0 is proportional to temperature, Fig. 2 underlines the differences in the value of the speed of sound throughout the system, particularly between the air inlets and the combustor. The average Mach number M_0 and speed of sound a_0 in the whole ramjet between the two acoustic boundaries and solely in the combustion chamber are provided in Table 1. A

notable increase of 37% of a_0 is induced by the combustor.

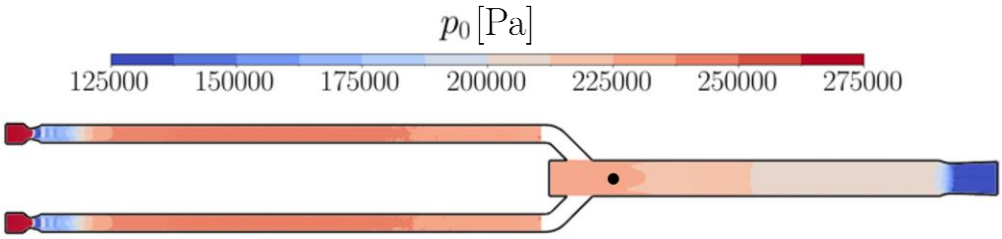

Fig. 3: Mean pressure field p_0 in the median plane along the z-axis. The black dot is the location of the pressure sensor mentioned in 2.2.

The mean pressure field p_0 is depicted in Fig. 3. The two acoustic boundaries of our system are discernable: the shock trains induced downstream of the sonic throats and the choked nozzle at the exit. An instantaneous representation of one of the inlet shock train on the median plane along the z-axis is proposed through a Mach number field in Fig. 4. The first normal shock is attached to the divergent section of the sonic throat and induces downstream lambda shocks separated from the walls. The recirculation zone above the shock train between the $M_0 = 1$ contour and the wall is pointed out by streamlines. The separation of the flow occurs in the divergent of the throat and is accentuated by the backward-facing step caused by the transition from a circular to a square section.

Due to pressure fluctuations originating from the combustion chamber, shock trains exhibit unsteady dynamics and the length of the train —i.e., the position of the last normal shock acting as an acoustic boundary— varies. This study does not focus on the precise characterization of shock train dynamics subjected to downstream perturbations, as a different spatial resolution and numerical methodology are required. Here, a mean acoustic length l_{a_0} of the Research Ramjet is estimated between the mean position of the isocontour $M_0 = 1$ at the extremity of the unsteady inlet shock trains and at the chocked nozzle and has a value of 2.45 m.

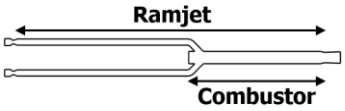

	M_0	a_0
Ramjet	0.27	622
Combustor	0.31	850

Tab. 1: Average acoustic properties in the Research Ramjet.

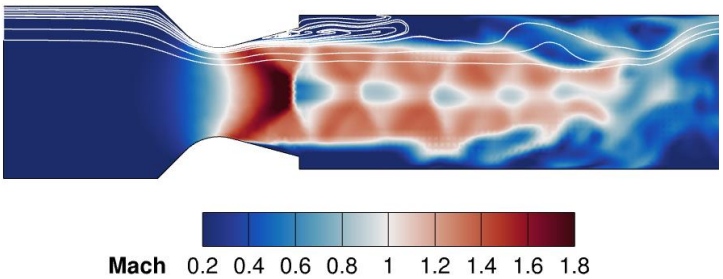

Fig. 4: Instantaneous field of Mach Number in one of the inlet shock trains in the median plane along the z-axis.

2.2. Temporal and spectral analysis

To characterize the acoustic field within the Research Ramjet, a temporal and spectral study of pressure fluctuations p_1 is conducted with a numerical sensor placed in the main combustion zone downstream the jet interaction zone, its location is represented by a black dot on Fig. 3. Its dimensionless temporal signal of pressure fluctuations p_1 normalized by the mean pressure p_0 is presented on the left side of Fig. 5. The temporal resolution of the signal is 2×10^{-5} s and the mean pressure at this location, also visible on Fig. 3, is $228\,200$ Pa. The pressure oscillation levels frequently exceed 20% of the mean pressure p_0 and even reach at multiple occasions 30%. These oscillation levels are significant and suggest a non-linearizable dynamics of our system, where pressure fluctuations cannot be neglected in comparison to the mean pressure.

A Fast-Fourier Transform (FFT) of the temporal signal of p_1 at the sensor is performed and presented on the right side of Fig. 5 on which the module of the Fourier Transform of p_1 is plotted against frequencies up to 1000 Hz. The spectral resolution of this signal is of 4.2 Hz. It should be noted that the liquid-fuelled configuration of the Research Ramjet exhibits high-frequency oscillations of the order of 4000 Hz which are identified as transverse modes. These high-frequency oscillations are not observed in the one-phase configuration [11,12] and are not explored in this study, which focuses on

the characterization of low-frequency longitudinal modes. Two distinct peaks are observed in the FFT: the highest amplitude is found at 126 Hz and the second one at 461 Hz.

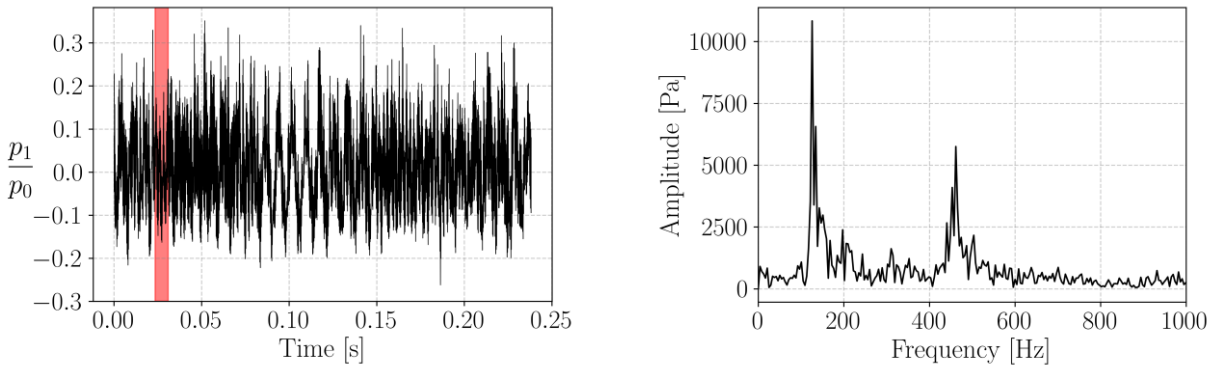

Fig. 5: Left: Temporal signal of pressure fluctuations p_1 normalized by the mean pressure p_0 at the pressure sensor. The red band is the time interval used in Fig. 6. Right: corresponding FFT of pressure fluctuations p_1 with a 4.2 Hz resolution.

To extend the temporal analysis, four instantaneous representations of p_1 in the median plane along the z-axis are presented in Fig. 6 to visualize the overall longitudinal acoustic behaviour of the system. The time interval between the first and last instantaneous are illustrated in the temporal signal by a red band on Fig. 5. The value range is set between -20000 and 20000 Pa to enhance the contrast between the two dynamics observed and described below. It should be noted that oscillations may reach higher levels, of the order of ± 30000 Pa, particularly in the dome region of the combustor and even more so in the shock trains oscillation zones.

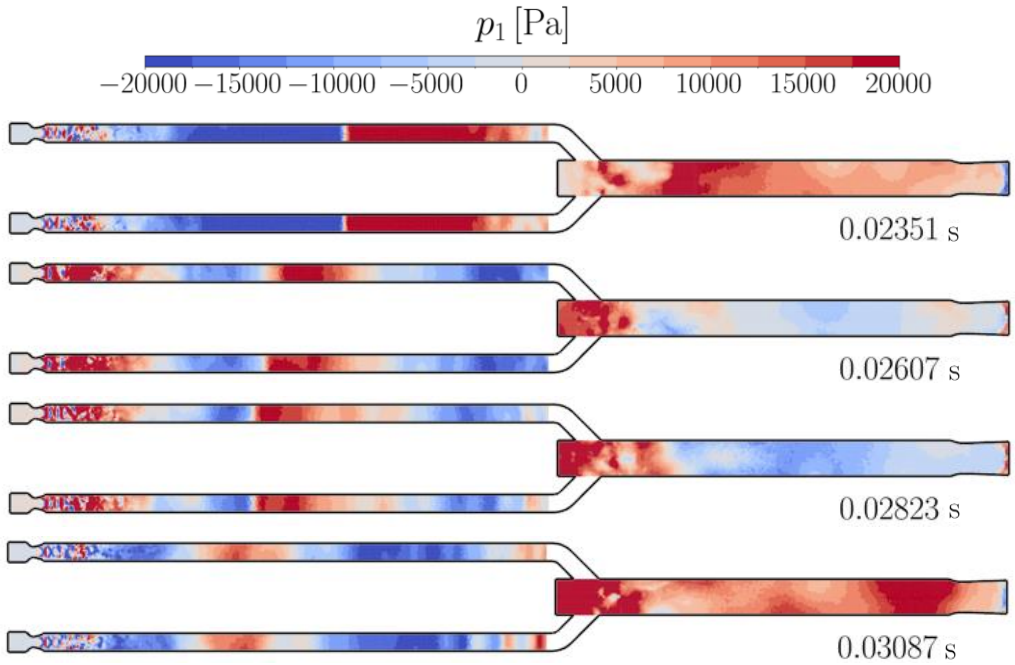

Fig. 6: Four instantaneous fields of pressure fluctuations p_1 in the median plane along the z-axis.

At the initial moment displayed at the top of Fig. 6, two bursts of pressure fluctuations can be highlighted. The first, having just exited the combustor, moves through the air inlets preceded by a depression. Its wave front travels upstream towards the shock trains. The second burst is visible in the combustion chamber where p_1 increases almost uniformly throughout the combustor.
At the second moment just below, the overpressure uniformly emanated from the chamber has traveled upstream and is now located at the center of the air inlets. Once again, another burst of p_1 is observed in the combustor but is confined to the upstream portion of the chamber leaving the last three-quarters of the combustor not affected by the p_1 increase.

At the third moment, 0.00216 s later (a period at 463 Hz), the exact same mechanism is observed: the burst of p_1 from the upstream quarter of the chamber from instant 2 has also traveled upstream in the air inlets and another burst emanates from the same portion. The wave resulting from the uniform pressure increase in the chamber observed at instant 1 is now interacting with the shock trains.
Finally, at the last moment 0.00736 s after instant 1 (a period at 136 Hz), the entire chamber is once again subjected to an almost uniform pressure increase, while p_1 waves from the upstream quarter of the chamber in previous moments traveled up the air inlets.
In light of these considerations, it appears that two dynamics of high-amplitude oscillation emission can be identified, both emanating from the combustor and propagating upstream in the air inlets: low frequency (≈ 130 Hz) oscillations emitted uniformly from the whole combustor intermittently accompanied by higher frequency oscillations (≈ 460 Hz) emanating from its upstream quarter.

For further analysis of the spectral distribution of p_1 within the Research Ramjet, a spectral map is displayed in Fig. 7. To generate it, pressure fluctuations along the y-axis were averaged at intervals of 1×10^{-2} m along the x-axis in the median plane according to the z-axis to create a one-dimensional representation of p_1. Following this, at each point, an FFT was computed resulting in a spectral map illustrating the spatial distribution of each frequency up to 1000 Hz along the ramjet. Here and later, the black dashed horizontal lines represent the ramjet boundaries whereas the red dashed lines represent the position of the average acoustic boundaries between both isocontour $M_0 = 1$ mentioned in 2.1. Notice that no pressure fluctuation is perceived upstream the isocontour $M = 1$ at the inlet nozzles throat, visible on Fig. 4.

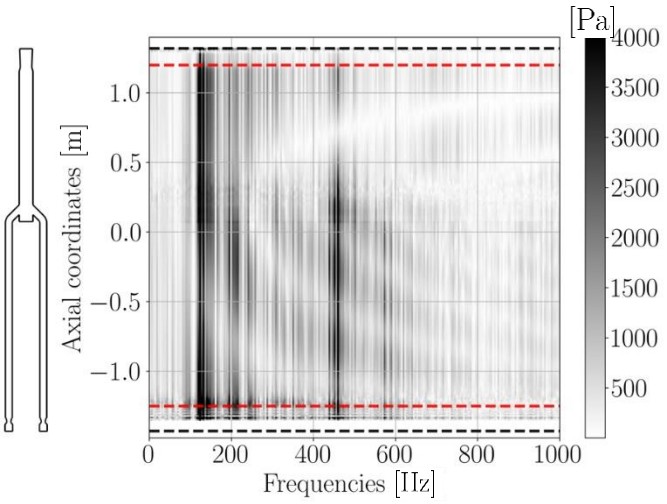

Fig. 7: Spectral map obtained by FFT of p_1 averaged along the y-axis in the median plane along the z-axis.

Both previously identified modes are also observed by the spectral map with a large spectral band around 126 Hz and a thinner band around 461 Hz. However, if those two modes stand out by their amplitudes, the multi-harmonic nature of the system is to be pointed out with the presence of other moderately excited band of frequencies around 220, 500 or 580 Hz and a background noise, which is often characteristic of complex systems.

As well as identifying the excited frequencies in the system, the spectral map also provides a spatial representation of theses excited frequencies. It allows to identify, for example, the pressure nodes made visible by zones of low to zero amplitude. A pressure node is particularly noteworthy for the 461 Hz mode at the center of the combustor whereas the predominant frequency band around 126 Hz does not seem to present any pressure node.

In the effort to deepen the analysis of the spatial structure of the two dominant pressure oscillation modes, the temporal reconstruction of pressure fluctuations filtered at the discrete value of the maximum of each excited band, respectively 126 and 461 Hz, was performed. It was achieved by applying a Discrete Fourier Transform (DFT) followed by an Inverse DFT (IDFT) at both frequencies as suggested by Eq. (2), on p_1 averaged along the y-axis.

$$p_{1,f} = \mathrm{Re}\left\{ \frac{2}{\left((T - t_0)/\Delta t\right)} \int_{t_0}^{T} p_1(t) e^{-i2\pi f t} dt \; e^{i2\pi f t} \right\} \tag{2}$$

The envelope of each $p_{1,f}$ is displayed on Fig. 8. On both of them the unsteady nature of the inlet shock trains is noticeable despite their three-dimensional with oblique shock dynamics and the averaged 1D post-processing used. The envelope of the dominant mode at 126 Hz confirms the observation previously made, $p_{1,126\,Hz}$ oscillates uniformly within the combustor. Its envelope does not have a defined pressure node while the pressure fluctuations do cancel out in the air inlet ducts. This is the result of a translation in space over time of p_1 indicating the presence of a global modal translation,

especially in the air inlet, impacting not only the location of pressure nodes but also the mode shape and its envelope. This translation is certainly the consequence of nonlinearities, high entropy fluctuations resulting from the shock train dynamics [23] and flame motions [24] as well as a non-uniform wave propagation speed in the system.

The same modal translation is particularly noticeable in the air inlet ducts for the lower amplitudes 461 Hz mode on the right of Fig. 8: pressure fluctuations do cancel out but since the mode shape translates over time, no pressure node is defined in this zone. However, this translation effect seems to be weak in the combustion chamber since a well-defined pressure node is located at its center, as observed in the spectral map on Fig. 7. Other studies have recorded similar modal structures in two side-dump ramjets [5,12]. In the one-phase configuration with a slightly different geometry of the Research Ramjet, Roux [12] observed its mode at 393 Hz to be a half-wave mode of the combustor. The envelope of $p_{1,461\,Hz}$ in the combustion chamber seems to confirm his observation, noting however a slightly different $p_{1,461\,Hz}$ dynamics from a half-wave mode in the dome and in the jet interaction zone.

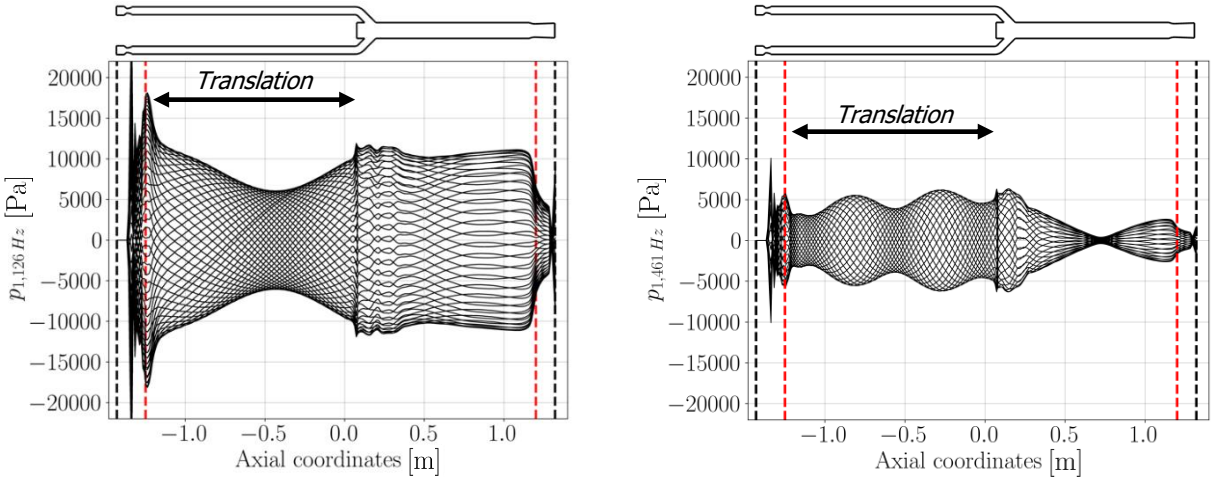

Fig. 8: Temporal evolution of the spatial structure of pressure fluctuations p_1 filtered by DFT and IDFT at Left: 126 Hz. Right: 461 Hz. Dashed lines: black: ramjet boundaries, red: average acoustic boundaries.

3. Predominant acoustic modes origin

An alternative to numerical simulation to enhance the understanding of the origin of the acoustic modes previously identified in the two-phase Research Ramjet is to decouple the acoustics-combustion loop by developing a reduced-order modeling of pure acoustics. In such models, the main focus is placed on the reproduction of the acoustic field in the combustion zone, crucial zone for a faithful thermoacoustic coupling between p_1 and $\dot{\omega}_{T_1}$. With this objective in mind and in order to corroborate the observation made by Roux [12] and in Section 2.2 of a combustor mode at 461 Hz, the origin of the two dominant modes is investigated by a linear acoustics approach with a whole ramjet and a combustor mode.

3.1. Linear acoustics reduced-order model

A linear acoustics reduced-order model allows the acoustic field to be decomposed into a sum of excited modes, enabling a decoupled and simplified analysis of their origin. It was demonstrated in Section 2.2 that the oscillation levels observed in the simulation suggested a non-linearizable dynamic of p_1, where fluctuations can not be considered negligible compared to the mean pressure. By developing a linear approach to model p_1, the limitations of the linear hypothesis will be evaluated in the case of the two-phase Research Ramjet.

Culick and Rogers [25] developed a one-dimensional model of the longitudinal acoustic pressure and velocity in a uniform mean flow field with constant cross-sectional area. Starting from the linearized balance equations without any source/loss and neglecting second order in fluctuation terms, the combination of the energy and momentum budgets leads to a homogeneous wave equation for the acoustic pressure with mean flow velocity u_0:

$$\frac{\partial^2 p_1}{\partial t^2} + 2u_0 \frac{\partial^2 p_1}{\partial x \partial t} + (u_0^2 - a_0^2) \frac{\partial^2 p_1}{\partial x^2} = 0 \tag{3}$$

A central assumption of harmonic fluctuations of the form $p_1 = \mathrm{Re}\{\hat{p}_1 e^{-i\omega t}\}$ is made which enables to express the Helmholtz equation:

$$(u_0^2 - a_0^2) \frac{\partial^2 \hat{p}_1}{\partial x^2} - 2i\omega u_0 \frac{\partial \hat{p}_1}{\partial x} - \omega^2 \hat{p}_1 = 0 \tag{4}$$

where $\omega = 2\pi f$ is the angular frequency. The solution of Eq. (4) is of the form:

$$\hat{p}_1 = P_+ e^{i\frac{k}{1+M_0}x} + P_- e^{-i\frac{k}{1-M_0}x} \tag{5}$$

where k is the wave number $k = \omega/a_0$. Eq. (5) combined with the harmonic fluctuations expression directly gives the pressure fluctuations p_1.

To close the model, it is necessary to define appropriate acoustic boundary conditions. For the modelling of p_1 within the entire Research Ramjet for the 126 Hz mode, later referred to as ramjet mode, a normal shock admittance A_I developed by Culick and Rogers [26] is employed as the inlet boundary to model the acoustic response of the shock trains. The formulation proposed for a separated flow in the nozzle in Eq. (6) is preferred due to the separation in the divergent section and recirculation zones highlighted in Fig. 4 and discussed in Section 2.1.

$$A_I = \frac{\frac{-2}{\gamma+1}\left(\frac{{M_{0_u}}^2+1}{{M_{0_u}}^2}\right) i\Omega - \frac{{M_{0_d}}^2}{{M_{0_u}}^2-1}}{\frac{4M_{0_u}}{\gamma+1}\frac{p_{0_u}}{p_{0_d}} i\Omega - \frac{1}{\gamma}\left(\frac{{M_{0_u}}^2}{{M_{0_u}}^2-1}\right)\frac{{M_{0_u}}^2-\left(\frac{\gamma+3}{2}\right)}{{M_{0_u}}^2-\left(\frac{\gamma-1}{2\gamma}\right)}} \tag{6}$$

The subscripts u and d in Eq. (6) represent, respectively, the average values upstream and downstream of the normal shock and γ the heat capacity ratio of the medium. The dimensionless frequency used in the inlet admittance is defined as $\Omega = \frac{\omega}{a_{0_d}}\left(\frac{1}{S}\frac{dS}{dx}\right)$ with S the cross-sectional area at the normal shock.

The axial placement of the normal shock admittance x_s in the model corresponds to the mean position of the last isocontour $M_0 = 1$ observed in the shock train, acting as an acoustic boundary. For the exit boundary condition, considering the low frequencies and the longitudinal nature of the mode under investigation here, the exit nozzle is modeled by a compact choked nozzle admittance [27,28,29] of the form: $A_O = M_0(\gamma - 1)/2$.

It was noted in Section 2.2, that the 461 Hz mode identified by numerical simulation may not be a whole ramjet mode but could originate from a natural combustor mode. To corroborate this observation on the mode origin through the reduced-order model, a different inlet boundary condition is chosen to model p_1 solely in the combustion chamber for the 461 Hz mode. An acoustic closed boundary ($u_1 = 0$) is adopted to model the dome wall impedance whereas the exit condition remains the identical.

The acoustic lengths established by simulation to model the ramjet and combustor modes are therefore different, being 2.45 and 1.12 m respectively. Similarly, due to influence of the combustion zone in the combustor, the mean values of the speed of sound and of the Mach Number in the combustor and in the whole ramjet differ. Detailed values for each of them in both mediums are presented in Tab. 1.

With the proper boundary conditions, the expressions of pressure fluctuations p_1 in both the whole ramjet for mode at 126 Hz and the combustor for mode at 461 Hz are respectively established:

$$p_{1,Ramjet} = \mathrm{Re}\left\{P_-[\beta e^{-2iQx_S} e^{iQx} + e^{-iQx}] e^{-iM_0 Qx} e^{-i\omega t}\right\} \tag{7}$$

$$p_{1,Combustor} = \mathrm{Re}\left\{P_-[e^{-2iQ_c x_c} e^{iQ_c x} + e^{-iQ_c x}] e^{-iM_{0_c} Q_c x} e^{-i\omega t}\right\} \tag{8}$$

with $\beta_I = (1 + A_I)/(1 - A_I)$ being the inlet reflection coefficient, A_I being the admittance of the inlet normal shock of position x_S. x_C is the position of the inlet closed boundary condition and $Q = k/(1 - {M_0}^2)$. In these expressions, P_- is an arbitrary fixed amplitude estimated to fit with numerical results.

Finally, relying on the linear approach of the model, total pressure fluctuation p_1 are modelled as the sum of pressure fluctuations from both excited modes n:

$$p_1 = \sum_n {p_1}_n(P_{-,n}, \omega_n, Q_n) \tag{9}$$

3.2. Acoustic mode structure

The frequencies of both modes obtained by the reference simulation and the linear reduced-order model are summarized in Tab. 2. The frequency of the first natural ramjet mode by the model differs by 10% from the simulation. However, the frequency of the first natural combustor mode calculated by the model is 347 Hz compared to 461 Hz by simulation, a 25% difference.

	Mode [Hz]	
	1	2
ZDES	126	461
Linear acoustic model	113	347

Tab. 2: Mode frequencies by linear acoustic model compared to ZDES.

A time step of 2.5×10^{-4} s is used in this model, sufficient to capture the lowest frequencies, with a total physical time of 0.6 s to ensure an adequate number of periods for finer resolution than in the simulation. To visualize the spatial distribution of both modes, a spectral map with a resolution of 3.3 Hz is presented in Fig. 9. The spectral band around 113 Hz and the spectral band associated with the combustor mode at 347 Hz in the combustion chamber are observed. One can notice that despite a 25% frequency difference, the latter exhibits a pressure node at the center of the combustor, exactly as in the simulation. Finally, the linear bi-harmonic nature of the spectral map differs from the multi-harmonic and noisy trends observed in Fig. 6. Indeed, apart from the calculated frequencies of both modes, no other frequencies are excited: the two modes sum up to generate the total pressure fluctuations p_1 without interacting with each other nor transferring energy to other frequencies.

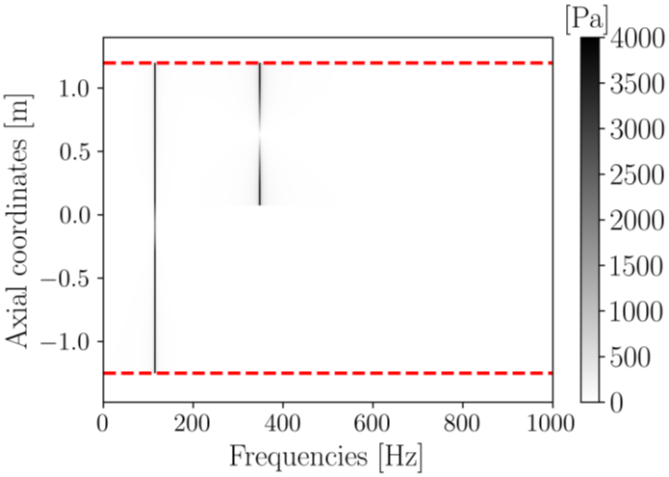

Fig. 9: Spectral map obtained by FFT of p_1 by linear acoustics model.

The temporal reconstruction of the spatial structure of both calculated modes by the linear model is depicted in Fig. 10, following the same method discussed in Section 2.2. The envelope of pressure fluctuations p_1 filtered at 113 Hz on the left of Fig. 10 shows a couple of differences compared to the mode envelop obtained by simulation.

The first difference is pressure fluctuations cancelling out at the center of the geometry at one point that weakly oscillates, giving the impression of a moderately established pressure node. This phenomenon, causing the overall envelope to resemble to a whole ramjet half-wave mode, shows the absence of the modal translation phenomenon observed in the simulation, in particular in the air inlet ducts, and its consequences on the structure of p_1.
The second difference with the simulation for the ramjet mode is the mode structure in the combustion chamber, a critical zone for the modelling of p_1 when studying the thermoacoustic coupling with $\dot{\omega}_{T_1}$. Pressure fluctuations in the combustor are not uniform as they are by simulation: the prediction of the model gives a 60% lower amplitude in the combustion zone compared to the chamber exit.

The envelope of the 347 Hz combustor mode by the linear model on the right of Fig. 10 is similar to the envelope obtained by simulation despite the 25% frequency difference. The pressure node prediction by the linear model is correct which is crucial for a potential prediction of thermoacoustic coupling with $\dot{\omega}_{T_1}$ in this zone. The linear acoustics model therefore appears to validate the observation made earlier on the origin of the 467 Hz mode by the simulation as being a natural acoustic chamber mode. However, it should be noted that the pressure node position is 7×10^{-2} m too far towards the dome which may be explained by the lower frequency of the calculated mode compared to the mode identified by simulation. Indeed, the jet interaction zone dynamics described in Section 2.2 may be responsible of a reduction of the acoustic length in the cavity, resulting in a frequency shift from the

natural acoustic mode and hence inducing the downstream displacement of the pressure node of the half-wave mode toward the nozzle exit in the simulation.

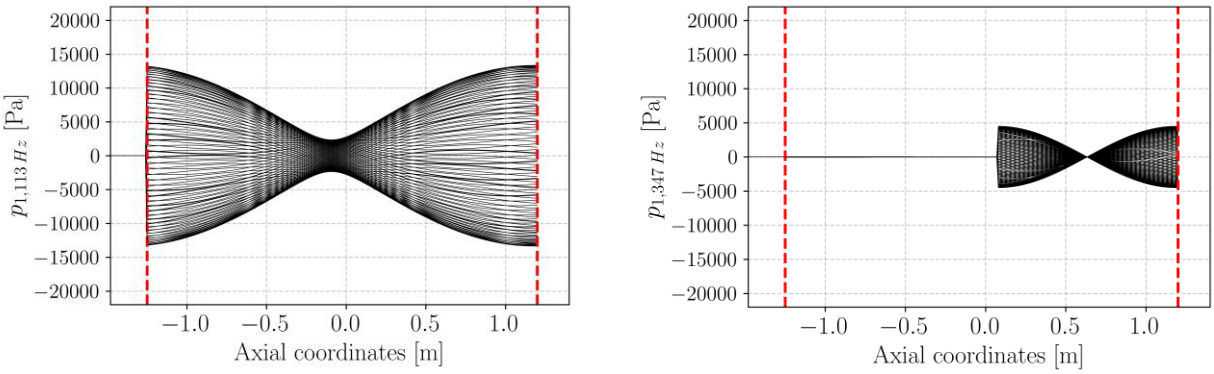

Fig. 10: Temporal evolution of the spatial structure of pressure fluctuations p_1 filtered by DFT and IDFT by linear acoustics model at Left: 113 Hz. Right: 347 Hz.

4. On the origins of the multi-harmonic dynamics and acoustic mode translation

A proposal is made here to introduce a correction to the linear acoustics model of Section 3, aiming to capture complex features observed in simulation, namely the multi-harmonicity of the p_1 spectrum and the modal translation. Their origins are investigated through the insertion of a translation in the model formalism.

4.1. *Ad Hoc* correction of the linear acoustics model

The correction developed is termed *'ad hoc'* as it directly stems from the modal translation observed by simulation and only aim at enhancing the comprehension of physical phenomena.

First, pressure fluctuations in the homogeneous wave equation Eq. (3) at mode *n* are decomposed as:

$$p_{1_n}(x,t) = \Upsilon_n(x)\, Z_n(t) \quad \text{with} \quad \frac{\partial^2 Z_n}{\partial t} = -\omega_n^2 Z_n \tag{10}$$

with ω_n the n-th angular frequency and Z_n the corresponding harmonic amplitudes. A translational motion is then introduced into the model, assuming the spatial component can be expressed as $\Upsilon(x) \rightarrow \Upsilon(x_T(x,t))$ where $x_T(x,t)$ represents the imposed translation. Developments lead to a second order differential equation acting with non-constant coefficients. A constraining hypothesis of a smooth evolution of these coefficients has to be made in order to solve the differential problem, whose general solution is the following:

$$\Upsilon_n = P_{-,n}\left(\beta_n e^{(\lambda_{1,n}+i\lambda_{2,n})(x-x_s)} + e^{(\lambda_{1,n}-i\lambda_{2,n})(x-x_s)}\right) \tag{11}$$

where reflection coefficients are $\beta_n = \beta_I$ for the ramjet mode and $\beta_n = 1$ for the combustor mode, corresponding to an acoustic closed condition. Expressions for $\lambda_{1,n}$ and $\lambda_{2,n}$are given by:

$$\lambda_{1,n} = \frac{-\frac{1}{2}\frac{\partial^2 x}{\partial t^2} - u_0\frac{\partial^2 x}{\partial t \partial x} - \frac{1}{Z_n}\frac{\partial Z_n}{\partial t}\left(\frac{\partial x}{\partial t} + u_0\right)}{\left(\frac{\partial x}{\partial t}\right)^2 + 2u_0\frac{\partial x}{\partial t} + ({u_0}^2 - {a_0}^2)}$$

$$\lambda_{2,n} = \frac{-\frac{1}{2}\frac{\partial^2 x}{\partial t^2} - u_0\frac{\partial^2 x}{\partial t \partial x} - \frac{1}{Z_n}\frac{\partial Z_n}{\partial t}\left(\frac{\partial x}{\partial t} + u_0\right) + \omega\left(\frac{\partial x}{\partial t} + \sqrt{2u_0\frac{\partial x}{\partial t}} + u_0 - a_0\right)}{\left(\frac{\partial x}{\partial t}\right)^2 + 2u_0\frac{\partial x}{\partial t} + ({u_0}^2 - {a_0}^2)} \tag{12}$$

The term $\partial x/\partial t$ is the translation velocity, homogenous to a variation of propagation speed, and needs to be modeled. For the combustor mode, only defined in the combustion chamber where modal translation is not impacting, $\partial x/\partial t = 0$ which is equivalent to the classical closed-nozzle admittance modeling of Section 3.

For the ramjet mode, simulation results showed that the modal translation is moderate in the vicinity of the inlet shock trains, minimal in the combustor and reaches a maximum amplitude in the air inlets

around $x = -0.5$ m. Roux [12] observed that the frequency of the wave reflected by the inlet shock trains, propagating back towards the combustor, was that of the first mode. Moreover, the latter is the predominant mode here and Fig.4 illustrated the strong interaction of pressure bursts emanating uniformly from the combustor with the inlet shock trains. Assuming their dynamics contribute to the modal translation observed, a sinusoidal oscillation at the ramjet mode frequency with an amplitude calibrated with the combustor mode amplitude is imposed to $\partial x/\partial t$. Therefore, an *ad hoc* parabolic shape in the air inlet ducts, oscillating at the ramjet mode frequency is chosen to model the translation term and is represented on Fig. 11:

$$\frac{\partial x}{\partial t} = P_{-,347\,Hz} \times F(x)\sin(\omega_{113\,Hz}\,t) \tag{13}$$

where: $P_{-,347\,Hz} = 2250$ Pa is the amplitude of the combustor mode fixed to match amplitudes observed by simulation. $F(x) = H(x_t - x) \times (fx^2 + gx + h)$ where $H(x_t - x)$ is the Heaviside function with x_t the position of the end of the translation fixed by observation of numerical results. f, g, h are the coefficients of the parabolic profile, respectively -8, 9.7 and 5.6.

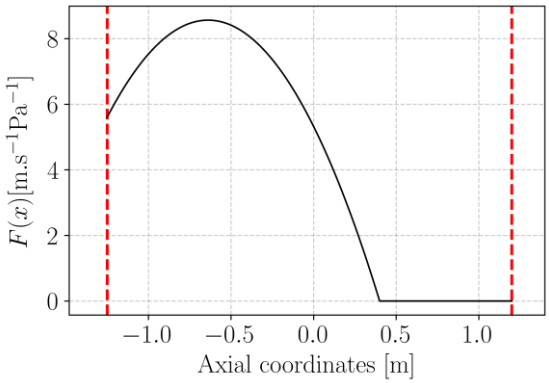

Fig. 11: Parabolic profile $F(x)$ of the translation velocity.

4.2. Excitation of new harmonics and acoustic mode envelope deformation

The spectral map obtained by the model with the introduction of a modal translation is presented in Fig. 12. The two modes calculated and considered by the model, namely the 113 and 347 Hz modes, are recovered. However, unlike the spectral map derived from the classical linear model in Section 3, new spectral bands emerge, indicating the excitation of additional frequencies in the system. The insertion of a translation velocity $\partial x/\partial t$ in the whole ramjet mode calculation has involved a multi-harmonic spectrum, approaching the spectral map obtained by simulation. New harmonics are excited for example at 220 Hz and 450 Hz. Similarly, a spectral band at 340 Hz is excited, especially in the air inlet ducts, very close to the 347 Hz chamber mode. The added insertion of a translation has therefore created an energy cascade towards new excited frequencies.

The principle of this energy cascade in the model is illustrated by a schematic in Fig. 13 and can be explained as follows: the amplitude of the combustor mode governs the amplitude of the translation velocity applied to the ramjet mode and oscillating at its frequency. Consequently, there is a one-way coupling between these two modes introduced by $\partial x/\partial t$ that induces an energy cascade towards new harmonics as visible in Fig. 12, including one with a frequency close to the chamber mode frequency.

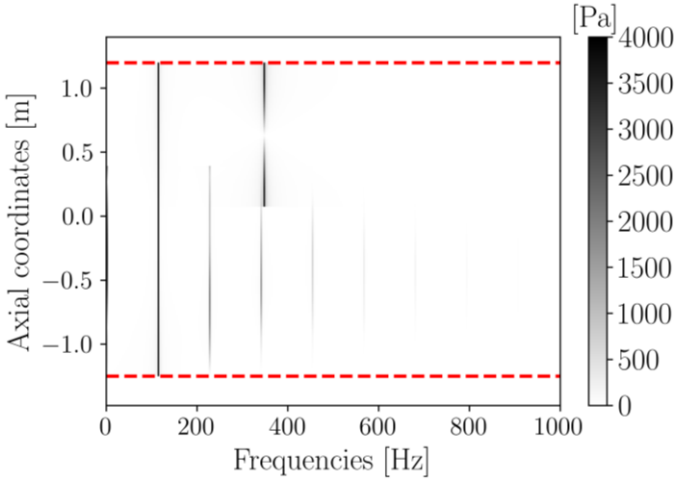

Fig. 12: Spectral map obtained by FFT of p_1 by linear acoustics model with the ad hoc translation

Finally, introducing a translation velocity in the model has caused a deformation of the envelope of the ramjet mode as visible in Fig. 14. The pressure node, which was too slightly oscillating around $x = -0.1$ m with the classical linear model, is not observed with the added translation. The mode envelope in the air inlets, where the translation velocity is added, is similar to the one observed in simulation. As for the combustion chamber portion, where the amplitude of $\partial x/\partial t$ is minimal, pressure fluctuations are more uniform, although not to the same extent as in the simulation. The introduction, in the linear formalism, of a translation velocity $\partial x/\partial t$ being homogeneous to a non-uniform and oscillating propagation speed in the air inlets has enabled the reproduction of a p_1 envelope analogous to the one obtained by simulation.

Capturing the simulation multi-harmonic dynamics with the *ad hoc* correction demonstrates that, in reality, there seems to be a coupling between the chamber mode and the ramjet mode in the liquid-fuelled Research Ramjet, modeled here by a translation driven by the amplitude of the combustor mode and applied to the ramjet mode.

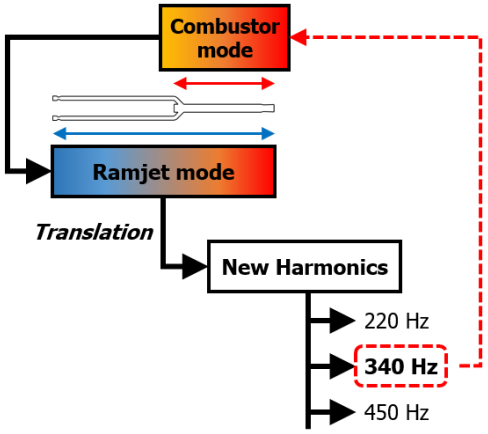

Fig. 13: Schematic of the one-way coupling between both modes resulting in a multi-harmonic spectrum.

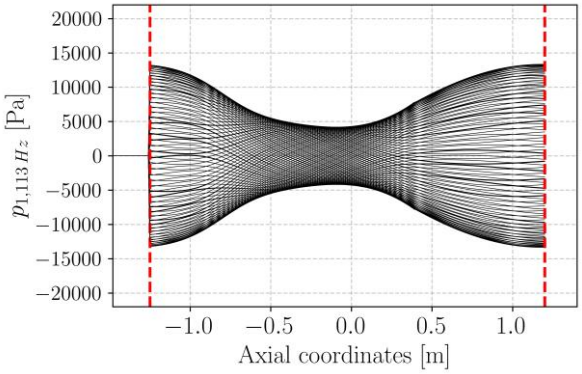

Fig. 14: Temporal evolution of the spatial structure of p_1 filtered by DFT and IDFT by linear acoustics model with *ad hoc* correction at 113 Hz.

Conclusion

The spectral but also structural characterization of the oscillation modes of p_1 is crucial, especially in a thermoacoustic study in which p_1 and $\dot{\omega}_{T_1}$ are strongly coupled, particularly in the combustion zone. This study aimed to characterize the acoustic field p_1 in the ONERA Research Ramjet in its liquid-fuelled configuration.

To achieve this, a 3D ZDES simulation was performed to describe the mean flow field and to conduct a temporal and spectral analysis of p_1. The observed oscillations levels suggested a non-linearizable dynamics of p_1. Two dominant modes were identified at 126 and 461 Hz but a spectral map revealed the multi-harmonicity of the system with other moderately excited spectral bands. The structure of both main modes suggested a natural eigenmode origin, with the first mode being a whole ramjet mode and the second one a combustion chamber mode. Also, a significant acoustic mode translation phenomenon in the air inlets was observed, causing a deformation of the mode envelope.

The origin of both excited modes was investigated relying on a reduced-order model for linear acoustics despite the oscillation levels reached in simulation. The model corroborated the hypothesis made on the modes origin by identifying the 126 Hz mode in simulation as a ramjet mode and the 461 Hz mode in simulation as a chamber mode. Therefore, the origin of excited modes in the Research Ramjet resides in natural geometric acoustic modes impacted by the unsteady heat release.

Nonetheless, the linearized model showed limitations in reproducing the multi-harmonic characteristic of the spectral map in Fig. 6 and in replicating the envelope of the first mode. An *ad hoc* correction, accounting for the modal translation, has been developed to investigate the origin of these phenomena observed by simulation. Introducing a translation velocity, homogenous to a non-uniform oscillating wave propagation speed, enabled to recover a multi-harmonic map with new excited frequencies. Furthermore, the envelope of the ramjet mode was also affected by the translation velocity, resulting in its deformation.

References

1. Rayleigh J.W.S.B.: The Theory of Sound Vol. 2. Macmillan (1896)
2. Culick, F.E.C.: Combustion Instabilities in Liquid-Fueled Propulsion Systems – an Overview. Combustion instabilities in liquid-fuelled propulsion systems, AGARD Conference Proceedings No.450 (1988)
3. Liewen, T.C.: Unsteady Combustor Physics. 2nd ed. New York, N.Y., Cambridge University Press (2021)
4. Ghirardo, G., Juniper, M.P. and Bothien, M.R.: The Effect of the Flame Phase on Thermoacoustic Instabilities. Combust. Flame 187, 165-184 (2018)
5. Crump, J. E., Schadow, K. C., Yang, V. and Culick, F. E.: Longitudinal combustion instabilities in ramjet engines identification of acoustic modes. J. Propul. Power, 2(2), 105-109 (1986)
6. Kim, S.D. and Jeung, I.S.: Numerical Simulation on a Reacting Flows of Coaxial Ramjet Dump Combustor with Liquid Fuel Injection. 42nd AIAA/ASME/SAE/ASEE Joint Propulsion Conference & Exhibit (2006)
7. Javed, A. and Chakraborty, D.: Numerical Simulations of Static Tested Ramjet Dump Combustor. J. Inst. Eng. India Ser. C. 99, 419-427 (2018)
8. Deppe, M.: Combustion Efficiency in a Dual-Inlet Side-Dump Ramjet Combustor. Thesis. Naval Postgraduate School, Monterey, California, USA (1984)
9. Le Pichon,T. and Laverdant, A.: Numerical Simulation of Reactive Flows in Ramjet Type Combustors and Associated Validation Experiments. AerospaceLab Journal 11-03 (2016)
10. Yang, V. and Culick, F.E.C.: Numerical Calculations of Pressure Oscillations in a Side-Dump Ramjet Engine. 22nd Aerospace Sciences Meeting (1984)
11. Reichstadt, S.: Etude du Mélange et de la Combustion Monophasique dans un Statoréacteur de Recherche (Study of Mixing and One-Phase Combustion in a Research Ramjet). PhD Thesis. Université de Pau et des pays de l'Adour, Pau, France (2007)
12. Roux, A.: Simulation aux Grandes Echelles d'un Statoréacteur (Large Eddy Simulation of a ramjet). PhD Thesis. Université de Toulouse, Toulouse, France (2009)
13. Deck., S.: Recent Improvements in the Zonal Detached Eddy Simulation (ZDES) formulation. Theor. Comp. Fluid. Dyn. 26, 523-550 (2012)
14. Refloch, A., Courbet, B., Murrone, A., Villedieu, P., Laurent, C., Gilbank, P., Troyes, J., Tesse, L., Chaineray, G., Dargaud, J.B., Quemerais, E. and Vuillot, F.: CEDRE Software. AerospaceLab Journal 2 (2011)
15. Murrone, A. and Villedieu, P.: Numerical Modeling of Dispersed Two-Phase Flows, AerospaceLab Journal 2 (2011)
16. Spalart, P.R., Deck, S., Shur, M.L., Squires, K.D., Strelets, M.Kh. and Travin,A.: A New Version of Detached-Eddy Simulation, Resistant to Ambiguous Grid Densities. Theor. Comp. Fluid. Dyn. 20, 181-195 (2006)
17. Fan, C.C., Xudong, X., Edwards, J.R., Hassan, H. and Baurle, R.: Hybrid Large-Eddy/Reynolds-Averaged Navier-Stokes Simulations of Shock-Separated Flows. J. Spacecraft Rockets 41.6, 897-906 (2004)
18. Franzelli, B., Riber, E., Sanjose, M. and Poinsot, T.: A Two-Step Chemical Scheme for Kerosene-Air Premixed Flames, Combust. Flame 157, 1364-1373 (2010)
19. Le Touze, C., Murrone, A. and Guillard, H.: Multislope MUSCL method for general unstructured meshes. J. Comput. Phys. 284, 389-418 (2015)
20. Van Leer, B.: Towards the ultimate conservative difference scheme. V. A second-order sequel to Godunov's method. J. Comput. Phys. 32, 101-136 (1979)
21. Ranz, W.E. and Marshall, W.R.: Evaporation from drops. Chem. Eng. Prog. 48, 3, 141-146

22. Pilch, M. and Erdman, C.A.: Use of Breakup Time Data and Velocity History Data to Predict the Maximum Size of Stable Fragments for Acceleration-Induced Breakup of a Liquid Drop. Int. J. Multiphas. Flow. 13, 6, 741-757 (1987)
23. Gnani, F., Zare-Behtash, H. and Kontis, K.: Pseudo-Shock Waves and their Interactions in High-Speed Intakes. Prog. Aerosp. Sci. 82, 36-56 (2016)
24. Klein, J.M, Gandilhon-Gunelle, A., Vincent-Randonnier, A., Genot, A. and Mura, A.: On the Invariance of Flame-Motion Induced Variations of the Generalized Disturbance Energy. Combust. Flame 251 (2023)
25. Culick, F.E.C. and Rogers, T.: Modeling pressure oscillations in ramjets. AIAA/SAE/ASME 16th Joint Propulsion Conference, AIAA-80-1192 (1980)
26. Culick, F.E.C. and Rogers, T.: The response of normal shocks in diffusers. AIAA J. 21, no 10, 1382-1390 (1983)
27. Crocco, L.: Supercritical gaseous discharge with high frequency oscillations. Aerotecnica 33, 46-53 (1953)
28. Zinn, B.T.: Longitudinal Mode Acoustic Losses in Short Nozzles. J. Sound Vib. 22, 93-105 (1972)
29. Marble, F.E. and Candel, S.M.: Acoustic Disturbance from Gas Non-Uniformities Convected Through a Nozzle. J. Sound Vib. 55, 225-243 (1877)